RESEARCH ARTICLE

A water flow model of the active crater lake at Aso volcano, Japan: fluctuations of magmatic gas and groundwater fluxes from the underlying hydrothermal system

Akihiko Terada · Takeshi Hashimoto ·
Tsuneomi Kagiyama

Abstract The first crater of Nakadake, peak of Aso volcano, Japan, contains a hot water lake that shows interesting variations in water level and temperature. These variations were discovered by precise, continuous observations of the lake independent of precipitation. We developed a numerical model of a hot crater lake and compared with observational data for the period from July 2006 to January 2009. The numerical model revealed seasonal changes in mass flux (75–132 kg/s) and enthalpy (1,840–3,030 kJ/kg) for the fluid supplied to the lake. The relation between the enthalpy and mass flux indicates that the bottom input fluid is a mixture of high- and low-temperature fluids. Assuming a mixture of high-temperature steam at 800°C and liquid water at 100°C, we evaluated the liquid and steam fluxes. The liquid water flux shows a seasonal increase lagging behind the rainy season by 2 months, suggesting that the liquid water is predominantly groundwater. The fluctuation pattern in the flux of the high-temperature steam shows a relation with the amplitude of volcanic tremor, suggesting that heating of the hydrothermal system drives the tremor. Consequently, precise observations of a hot crater lake represent a potential method of monitoring volcanic hydrothermal systems in the shallow parts of the volcanoes.

Keyword Aso volcano · Hot crater lake · Hydrothermal system · Groundwater · Volcanic tremor

A. Terada (✉) · T. Kagiyama
Aso Volcanological Laboratory, Kyoto University,
5280 Kawayo, Minami-Aso,
Kumamoto 869-1404, Japan
e-mail: terada@ksvo.titech.ac.jp

T. Hashimoto
Institute of Seismology and Volcanology, Faculty of Science,
Hokkaido University,
North 10 West 8, Kita-ku,
Sapporo 060-0810, Japan

Present Address:
A. Terada
Volcanic Fluid Research Center, Tokyo Institute of Technology,
641-36 Kusatsu,
Gunma 377-1711, Japan

Introduction

Hot crater lakes on active volcanoes generally overlie magma–hydrothermal systems. The water level and temperature of such lakes can exhibit changes in response to volcanic activity (Brown et al. 1989; Hurst et al. 1991). Based on analyses of chemical components, seismicity, and heat budgets, some crater lakes are regarded as a constituent part of their hydrothermal systems (e.g., Poás volcano in Costa Rica: Rowe et al. 1992; Stevenson 1992; Kusatsu-Shirane volcano in Japan: Ohba et al. 1994). Laboratory experiments investigating changes in water level at Inferno Crater Lake in the Waimangu Geothermal Field, New Zealand, revealed that the cyclic changes in water level were caused by periodic thermal instability in porous media (Vandemeulebrouck et al. 2005). Because volcanic activity such as continuous tremor can occur as a result of steam-water flow instability (Iwamura and Kaneshima 2005), monitoring the hydrothermal system beneath an active crater would provide information useful for understanding the mechanisms of these phenomena and for forecasting volcanic activity.

Nakadake, an active crater in the Aso caldera, central Kyushu, Japan (Fig. 1a), is one of the most active volcanoes in Japan in terms of the persistent release of
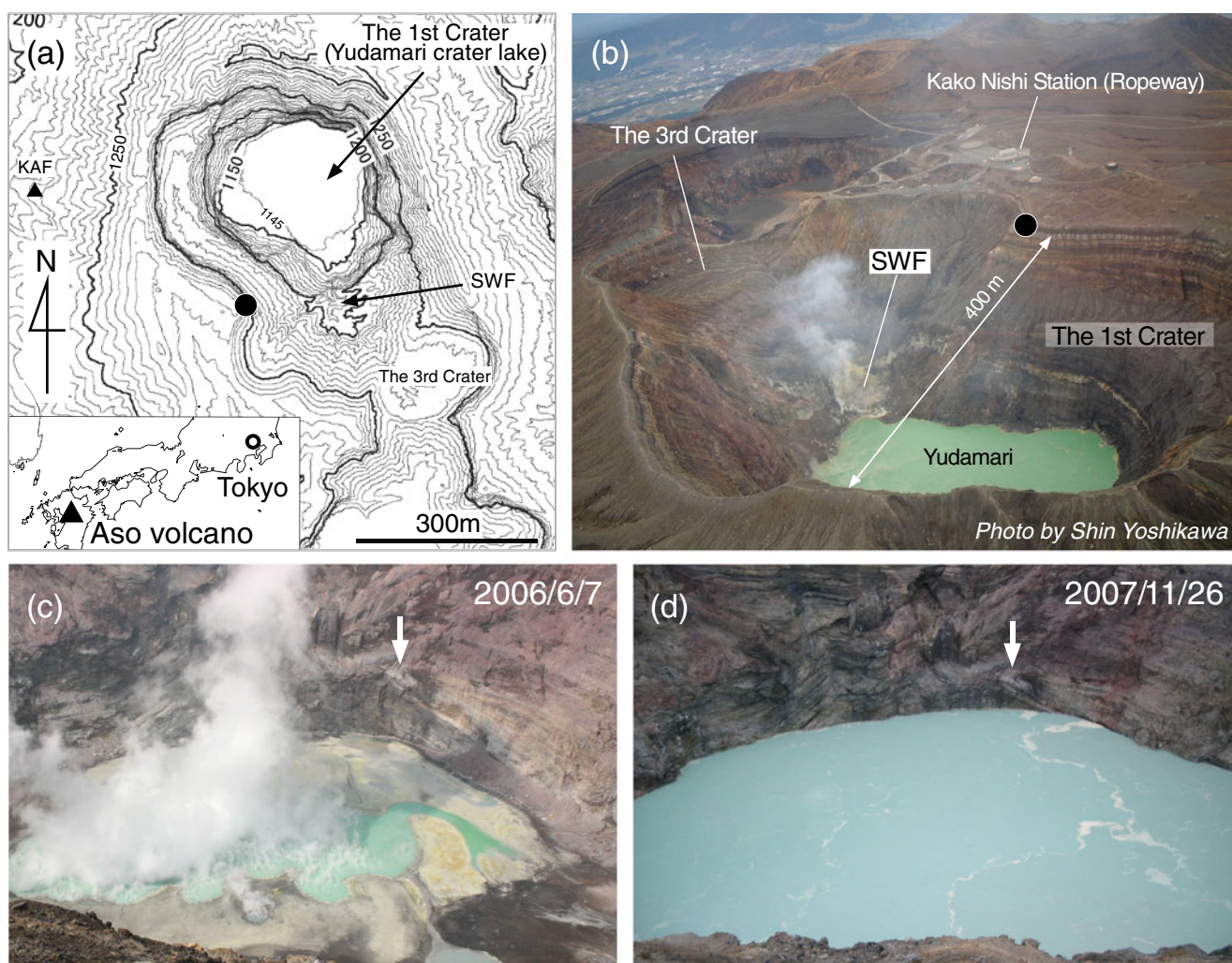
Fig. 1 **a** Location map (*inserted figure*) and topographic map of the Nakadake Craters based on a digital surface model (1-m mesh) obtained from an airborne survey using a laser scanner in April 2004 (data are from Kokusai Kogyo Co., Ltd.), when most of the lake bottom was visible (Terada et al. 2008). *Solid lines* are topographic contours at intervals of 5 m. The *closed circle* indicates the location of the automatic image-recording system. A drill hole for ground temperature measurements is located at the *triangle* (*KAF*, Sudo and

Hurst 1998). *SWF* means south wall fumaroles. **b** Aerial photograph of the Nakadake Craters. Photographs are shown of the first crater of Nakadake taken on 10 June 2006 (**c**) and on 26 November 2007 (**d**). To assist with orientation, the whitish portion of the wall marked by the *white arrow* in (**c**) is identical to that marked in (**d**). Both photographs were taken from the top of the crater wall (*closed circle* in **a**)

volatiles and thermal energy. Throughout most of the recent non-eruptive periods at Nakadake, a large amount of volcanic gas (typically 200–400 tonnes/day of SO_2; monthly report of the Japan Meteorological Agency, hereafter JMA) has been continuously emitted. The first crater of Nakadake contains a hot lake, locally called Yudamari (Fig. 1b), that is more than 200 m in diameter. During a recent calm period, the lake's temperature typically remained at 60–70°C.

Monthly reports by JMA suggest that the water level and temperature of Yudamari are related to volcanic activity. The water level shows a rapid fall preceding an eruptive period. The disappearance of the lake water may be followed by the emergence of a red-hot glow at the crater

bottom or wall, by phreatic or phreatomagmatic explosions, and, finally, by Strombolian activity that typically lasts for several months. The lake then re-forms with the return of eruptive quiescence. Similar drastic changes in lake water have also been reported at Poás in Costa Rica (Brown et al. 1989; Rowe et al. 1992) and for Ruapehu in New Zealand (Hurst et al. 1991) and are probably caused by changes in the input of volcanic fluid to the crater bottom.

At crater lakes such as Yudamari, most of the thermal energy and mass injected into the lake bottom is intercepted by the lake rather than passing directly to the atmosphere (Stevenson 1992). Therefore, precise observations and analyses of a hot crater lake such as Yudamari could reveal even slight changes in the input of volcanic fluids

originating from the underlying hydrothermal system. In the present study, we develop a numerical model of a hot crater lake and apply it to the observational data obtained at Yudamari while evaluating the nature of temporal variations in mass flux and the specific enthalpy of the volcanic fluid supplied through the lake bottom. Based on the results of this analysis, we propose a model of the water flow from the hydrothermal system beneath Yudamari, and we discuss its relation to volcanic activity at Aso volcano.

Observations

Temporal changes in lake level

Direct monitoring of the lake water at Yudamari is made difficult by the steep topography (Fig. 1b) and high concentrations of SO_2 gas. The recent development of a high-resolution digital surface model (DSM) and installation of a commercial digital camera (Terada et al. 2008) has enabled precise and continuous monitoring of Yudamari from July 2006 to January 2009.

Temporal changes in water level at Yudamari are shown in Fig. 2a, as calculated from analyses of the high-resolution

images. We tried to measure the water level each day because the changes in water level were generally slow, except during periods of heavy rain. The lake level showed a marked increase from June to July 2006, coinciding with the rainy season. This rapid rise during the rainy season has been observed every year (gray arrows in Fig. 2).

A comparison of trends in lake level (Fig. 2a) and precipitation (Fig. 2b) reveals that periods of mild increases in lake level (period C in Fig. 2, +5.4 cm/day; period D, +2.7 cm/day) show no direct correlation with precipitation. Periods B, E, L, and Q only include data for the first and final days of each period because of technical problems and the obscuring effects of steam within the crater. Based on the magnitude of changes in lake level, we define plateau periods (change of less than ±1 cm/day: periods A, F, H, J, and O in Fig. 2) and periods of gradual decrease (between −1.4 cm/day and −2.7 cm/day: periods G, I, K, M, N, P, and R) in addition to periods with a mild increase (C and D).

Lake surface area and volume

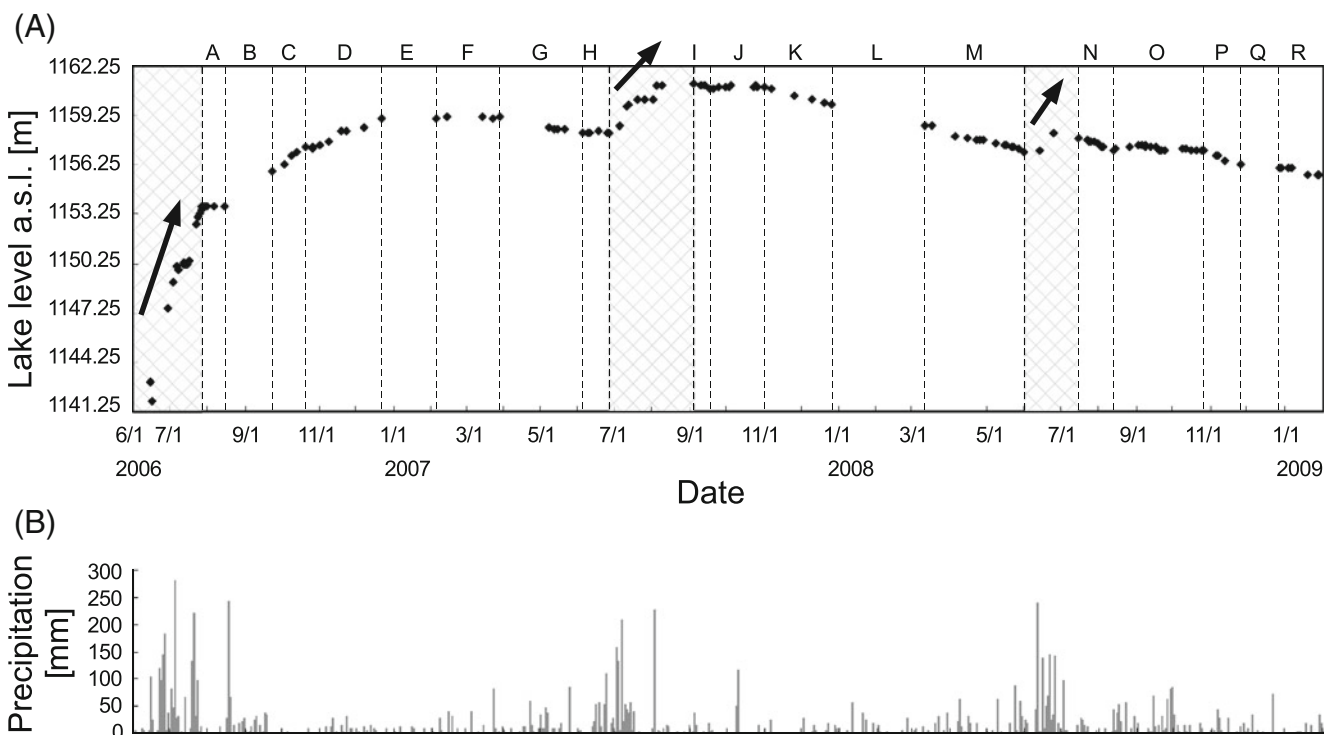The lake surface area is one of the key parameters in estimating the discharge rates of heat and mass across the

Fig. 2 a Temporal changes in water level at Yudamari Crater Lake, as estimated from high-resolution images of the inner wall and a digital surface model. The periods indicated by three meshes represent rainy seasons. The elevation of 1,141.25 m above sea level (a.s.l.) corresponds to the minimum altitude of the lake floor, as observed in April 2004 (Terada et al. 2008). We identified 18 distinct periods in the time series of water level (labeled A–R) based on trends in water level change. b Daily precipitation observed at the Aso Weather Station, located 1.2 km west of the first crater

lake surface (Pasternack and Varekamp 1997). The lake surface area S (m^2) is calculated as a function of water level h (m) based on the DSM (1-m mesh) with an average accuracy of 10–30 cm (Terada et al. 2008). Temporal changes in the lake surface area (Fig. 3a) show that it maintains a near-constant area of 46,000 m^2, reflecting nearly vertical sides of the crater walls (Fig. 1a).

Temporal changes in water volume (open squares in Fig. 3b) are calculated by the relation between water level h (m) and water volume V (m^3) as determined from the DSM (Terada et al. 2008). The Yudamari crater lake, which contained less than 10,000 m^3 of water in June 2006, grew significantly from July 2006 (Fig. 1c) to July 2007 (Fig. 1d). The open squares in Fig. 3b overestimate the volume because lacustrine sediments accumulate on the lake bottom when it is covered by water. Assuming sediment accumulates at the very rapid rate of 2 m/year (0.55 cm/day; Miyabuchi and Terada 2009), it is possible to calculate the actual water volume (*closed squares* in Fig. 3b).
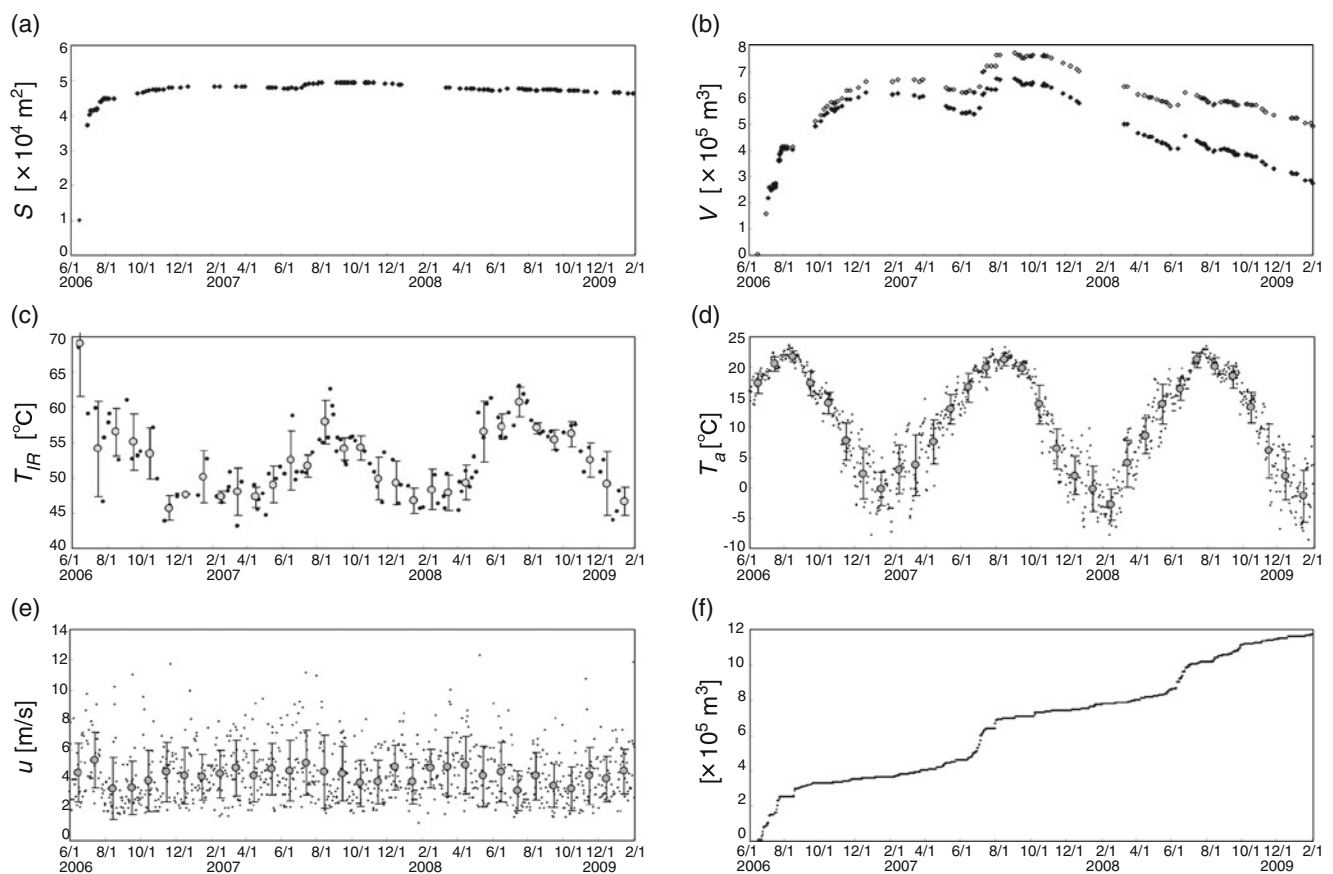
Water temperature

Figure 3c shows temporal changes in the temperature of the surface water, as measured by infrared (IR) thermometry from the top of the crater wall (closed circle in Fig. 1a), denoted as T_{IR} °C. JMA performs temperature observations at the lake several days per month. The surface temperature of Yudamari shows an annual cycle, even allowing for the large scatter in the data (Terada et al. 2008).

The temperature T_{IR} °C is generally lower than the actual temperature due to the absorption effect of water vapor. To overcome this problem, we calibrated T_{IR} °C based on occasional in situ temperature measurements of the lake water. Using wireless thermometers attached to a telemetry buoy, water temperatures at a 40 cm depth were recorded from April to August 2007 (Terada and Yoshikawa 2009). The IR thermometer repeatedly measured T_{IR} °C, but only when no steam filled the first crater, at which time the apparent water temperatures are nearly uniform over the

Fig. 3 a Computed lake surface area (S) and **b** water volume at Yudamari crater lake (V). *Open circles* represent results calculated using the relation (Terada et al. 2008) and lake level data shown in Fig. 2a. *Closed circles* in Fig. 3b indicate results for which the volume of sulfur accumulation on the lake bottom was deducted from lake volume (as indicated by open circles in Fig. 3b). See text for details. **c** Apparent temperature of the lake surface as measured by IR thermometry (T_{IR}), operated by the Japan Meteorological Agency. **d** Air temperature (T_a) and **e** wind speed (u) measured at Aso Weather Station (AWS). *Small dots* represent measurements; *gray circles* are monthly means with one standard deviation. **e** Cumulative curve of precipitation at AWS

entire lake surface. Figure 4 shows the relationship between apparent water surface temperature T_{IR} (as measured by the IR thermometer) and water temperature T (as measured in situ from a buoy). This suggests that T can be empirically obtained as $T_{IR}+8.3°C$.

Numerical model of hot crater lakes

To evaluate the heat and water budgets of hot crater lakes, a so-called box model is applied, taking into account the terms directly derived from observable variables (e.g., precipitation, surface evaporation, and radiation) and non-observable terms (e.g., volcanic input from the lake bottom and seepage). In some cases, the inputs of heat and mass from the lake bottom are estimated based on the observation data (Hurst et al. 1991; Rowe et al. 1992; Brantley et al. 1993; Ohba et al. 1994; Pasternack and Varekamp 1997; Rouwet et al. 2004). Saito et al. (2008) applied the box model to obtain a preliminary result for Yudamari; however, the observation data (e.g., lake water volume, temperature, and atmospheric conditions) contain large uncertainties. Based on the precise monitoring at Yudamari, we estimated the temporal variations in flux and enthalpy from the lake bottom using the numerical model outlined below.

Basic assumptions

An essential assumption of this study is that fumaroles and/or hot water fountains exist at the crater bottom. These vents are covered by lake water, meaning all the mass and energy injected from the lake bottom are absorbed by the lake water. For simplicity, it is assumed that the lake water is well mixed and thus, the water temperature is homogeneous.

This study considers a closed lake with no surface runoff outlets. We define the system at Yudamari crater
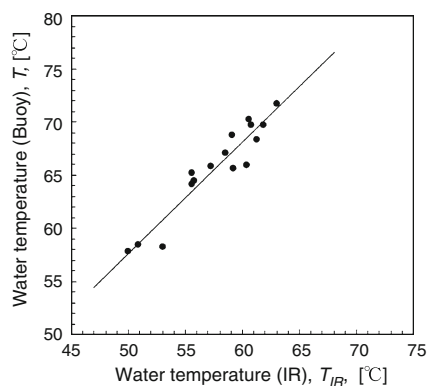

Fig. 4 Relationship between apparent water surface temperature (T_{IR}) and water temperature at 40 cm depth (T). The line of best fit was calculated by the least squares method

lake as depicted in Fig. 5. The lake's water is supplied by fluid injection at the lake bottom and by precipitation inflow. The water is lost by evaporation from the lake surface and by seepage through the lake bottom. Enthalpy is added to the lake in the form of fluid supply from the lake bottom and from precipitation as well as solar and atmospheric radiation, and it is lost by evaporative, conductive, and radiative heat transfer from the lake surface to the atmosphere and by seepage through the lake bottom. Conductive heat flow through the crater bottom or wall is ignored. This situation corresponds approximately to the model proposed by Stevenson (1992).

Formulation

The total mass flux of fluid input from the lake bottom comprises vapor, hot water of volcanic origin, and groundwater. Hereafter, this fluid is referred to as "bottom input fluid" and its flux is denoted as m [kg/s]. Using V as the volume of the lake water as a function of lake level h and its mean density ρ (Table 1), the conservation of mass for the lake water is expressed as

$$\rho \frac{dV(h)}{dt} = m - \frac{\varphi_e S(h)}{L} - m_b + pS_c \quad (1)$$

where S is the lake's surface area as a function of h, L is the latent heat of the water (Table 1), φ_e is the evaporative heat flux described in the Appendix, m_b is the seepage flux through the lake bottom, p is the precipitation in kg/(m^2 s), and S_c is the effective catchment area. The second term on the right-hand-side represents the evaporative mass flux from the lake surface, which depends on atmospheric conditions such as temperature T_a, vapor pressure e_a, wind speed u, and ambient pressure (see Appendix).

The conservation of total energy of the lake water is expressed as

$$\rho C_{pw} \frac{d}{dt}[TV(h)] = Hm - \Phi S(h) - m_b C_{pw} T + pS_c C_{pw} T_a \quad (2)$$

where T is the bulk water temperature and C_{pw} is the specific heat of the lake water (Table 1). We define H [J/kg], the bottom input enthalpy per unit mass, as the average enthalpy among the vapor, hot water, and groundwater injected through the lake bottom. The second term, Φ, on the right-hand side, is the heat flux from the lake surface, which is the sum of heat fluxes due to evaporation φ_e, conduction φ_c, and radiation φ_r, as described in the Appendix.

The function Φ depends mainly on $T_s°C$, the surface temperature of the lake. Due to the skin effect (a slight decrease in water temperature in the boundary layer at the
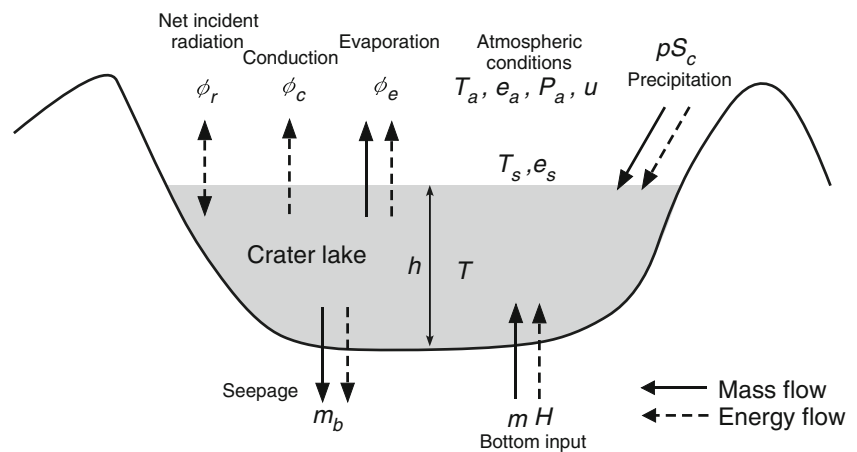
very surface of the lake), the surface temperature T_s is typically several degrees cooler than T, the temperature of the bulk water. Based on field observations at Kawah Ijen in Indonesia, Oppenheimer (1997) investigated this type of surface cooling and obtained the following empirical relation as a function of u, the wind speed over the lake:

$$T - T_s = 1.12 + 0.16u \qquad (3)$$

In the third term of Eqs. 1 and 2, following Darcy's law, we assume that seepage flux through the lake bottom is proportional to the lake's depth and area:

$$m_b = i\rho h S \qquad (4)$$

where i is an empirical constant.

Application to Yudamari crater lake

Methodology

We analyze 18 distinct periods in the time series of water level (labeled A–R in Fig. 2) with an assumption of constant bottom input of H and m during each period. We ignore the rainy season (June and July) because precipitation input during the rainy season is less certain than that of periods of A–R.

Using a fourth-order Runge–Kutta scheme (time step of 10 min), water level h and temperature T are computed as a function of time. Comparing the calculated values of T and h with the observation data (Figs. 2a and 3c), the optimal values of H and m are determined by minimizing the root mean square of the residuals. To compute T and h, it is necessary to know the initial water temperature T_0 and level h_0 for each period. We set a water level, as measured on the first day, for h_0 in each period. However, observations of the water temperature were not carried out on the first day of each period. In such cases (periods B–G, I, and N–R), T_0

was calculated by linear interpolation using temporally adjacent temperature measurements.

Parameter settings

The water surface area S and volume V are given as a function of h (Terada et al. 2008). Atmospheric conditions such as air temperature T_a (Fig. 3d), vapor pressure e_a, and atmospheric pressure are considered the daily mean values measured at the Aso Weather Station (AWS, operated by JMA), which is located 1.2 km west of the first crater.

The wind speed u (Fig. 3e) obtained at AWS must be applied with care to the wind speed in the crater because the effective wind speed on the lake appears to be systematically reduced by the sheltering effect of the topography (Fig. 1). Consequently, the wind speed over the lake is assumed to be 75% of the wind velocity measured at AWS. We assess the uncertainty in the estimated wind speed below (see Results).

Precipitation around the crater can be estimated from the AWS data multiplied by a factor of 1.1 (Terada et al. 2008). By comparing the changes in the water volume of Yudamari and the precipitation, the equivalent catchment area S_c is estimated to be 110,000 m^2 (Terada et al. 2008). Based on the S_c values and the precipitation data recorded at AWS, the cumulative precipitation inflow is shown in Fig. 3f.

To determine the empirical constant of the seepage rate i, we obtained data from the literature on the seepage flux, surface area, and mean depth of various crater lakes. Figure 6 shows that the seepage flux correlates with the equivalent volume (the product of the lake's surface area and mean depth), except for the case of Poás. According to the empirical relation in Fig. 6, the seepage flux is estimated to be roughly 25 kg/s assuming a lake surface area of 46,000 m^2 and depth of 15 m, which are representative values for Yudamari. Then, i is estimated to be 3.62×10^{-8} (1/s). Because the seepage flux is potentially an important factor in estimating the bottom input

Table 1 Definitions of abbreviations

h	Lake depth, m
S	Lake surface area, m^2
S_c	Effective catchment area, m^2
V	Lake volume, m^3
T	Temperature of lake water, °C
T_s	Temperature of lake surface water, °C
T_a	Air temperature at 2 m above a lake surface, °C
T_{vs}	Virtual temperature at the lake surface, K
T_{va}	Virtual temperature at 2 m above a lake surface, K
H	Specific enthalpy of the bottom input fluid, J/kg
C_{pw}	Specific heat of lake water at 50°C, 4,182 J/kg/K
L	Latent heat of the water at 50°C, 2.38210 J/kg
m	Mass flux of the bottom input fluid, kg/s
m_b	Flux of water seepaging through the lake bottom, kg/s
ρ	Water density, 1,000 kg/m^3
e	Vapor pressure, Pa
u	Wind velocity at 2 m above the lake surface, m/s
p	Precipitation rate, $kg/m^2/s$
Φ	Total heat flux from the lake surface, W/m^2
φ_e	Evaporation heat flux from the lake surface, W/m^2
φ_c	Conduction heat flux from the lake surface, W/m^2
φ_r	Net radiation heat flux from the lake surface, W/m^2
R_{lake}	Long-wavelength radiation from the lake surface, W/m^2
R_{sun}	Short-wavelength solar radiation to the lake surface, W/m^2
R_{atm}	Long-wavelength radiation to the lake surface, W/m^2
C	Constant, 61 Pa/K
λ	Constant, 0.027 $W/m^2/Pa/K^{1/3}$
b_0	Empirical constant, 0.032 $W/m^2/Pa/(m/s)$
B_o	Bowen ratio
C_1	Average cloud cover, $W/m^2/K$
l	Latitude of lake
i	Empirical constant for seepage rate, 1/s
f	Empirical constant for catchment area
ε	Emissivity of the lake surface, 0.97
σ	Stefan-Boltzmann constant, 5.67×10^{-8} $W/m^2/K^4$
Subscripts of H and m	
v	Value in steam at 800°C
w	Value in liquid water at 100°C

mass m, we assess the validity of seepage flux based on the measured SO_2 flux (see Discussion).

Results

Comparisons of calculations and observations

Optimal results are shown for a time of increasing water level (period D; Fig. 7a), unchanging water level (period J; Fig. 7b), and decreasing in water level (period M;

Fig. 7c). The values of air temperature, wind speed, and precipitation applied to the calculations are shown in Figs. 7 [2] and [3]. The computed water temperatures show some variations, whereas the bottom input mass and enthalpy are constant. Cyclic changes in water temperature with a typical term of several days are related to variations in wind speed (Fig. 7 [3]). Wind acts to enhance forced convection (see Appendix), causing enhanced evaporation and, consequently, a decrease in temperature. Long-term variations (2–4 weeks) in water temperature are caused by changes in air temperature. If
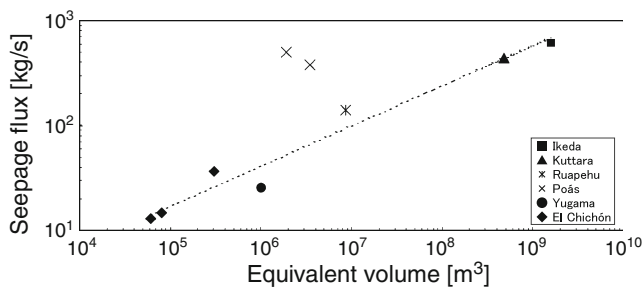
Fig. 6 Empirical relation between seepage flux and equivalent volume (the product of lake surface area and mean depth). The data (excluding Poás) are fitted by the least squares method (*dashed line*). Seepage flux at Yugama, Kusatsu-Shirane volcano (Ohba et al. 1994), are averaged between 1988 and 1993. Kuttara (4 km in diameter) and Ikeda (3 km in diameter) are caldera lakes in Japan (see Abe 1972; Nakao et al. 1967). In the cases of Poás (Rowe et al. 1992) and El Chichon (Rouwet et al. 2004), the lake level and surface area show marked temporal changes. We therefore selected data for periods in which the lake surface areas were stable, when the budget analyses were performed (Poás: March 1978 to October 1984 and May 1986 to January 1988; El Chichon: 20 May 1995–7 April 1998, 20 November 1998–10 August 1999, and 22 January 2001–19 April 2001). To evaluate seepage flux through the lake bottom at Ruapehu, we subtract the observed overflow flux (Hurst et al. 1991) from the sum of seeping and overflowing water flux estimated by Stevenson (1992). Here, we show the yearly averaged data in 1984 because the observed overflow flux is nearly stable throughout this year in which the volcanic activity was calm

the air temperature rises, free convection is restrained (see Eq. 6), and consequently, the water temperature rises. Changes in air temperature within a period of several days do not significantly influence water temperature, given the large heat capacity of lake water.

We tested the sensitivity of the optimizations for mass and enthalpy by varying these factors in turn. The dashed lines in Fig. 7 [1] represent water level calculated using the optimal mass (±10%) and optimal enthalpy. In period D, the water level on the final day of the period ranges up to 60 cm, which is greater than the measurement accuracy of 10–20 cm. Using the optimal enthalpy (±10%) with optimal mass, we computed the water temperature, as shown by the dashed lines in Fig. 7 [2]. The water temperature shows a systematic shift of 3°C in comparison with the optimal temperature results. Therefore, we consider that the bottom input mass and enthalpy are sensitive to calculations of water level and temperature. We thus consider that the model largely explains the observed data on water level and temperature using optimal mass and enthalpy with uncertainties of less than ±10%.

Mass and energy budgets for Yudamari crater lake

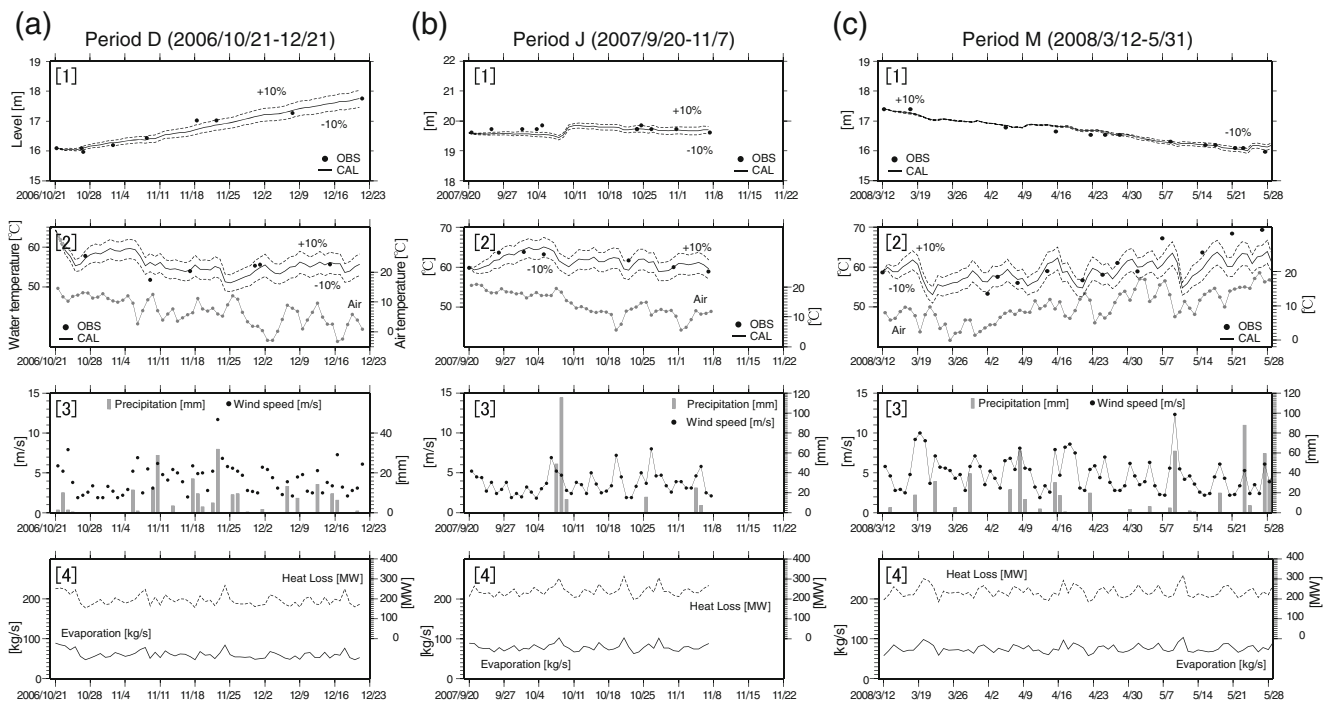The computed mass and energy budgets for the representative periods D, J, and M are summarized in

Fig. 7 Computed *[1]* water level and *[2]* temperature as a function of time for Yudamari crater lake at Aso volcano. *Solid curves* show the calculation results using optimal *m* and *H*, giving minimum residuals. *Dashed lines* in *[1]* indicate changes in level using ±10% of optimal *m*, whereas the other lines were calculated using optimal *H*. In the same way, the *dashed lines* in *[2]* indicate changes in water temperature using ±10% of optimal *H*, whereas other lines were calculated using optimal *m*. Daily mean air temperature is shown in *[2]*, and wind speed and daily precipitation are shown in *[3]*. Computed total heat loss (*dashed lines*) and evaporative mass (*solid lines*) are shown in *[4]*. The columns of the panels show data for **a** period D, **b** period J, and **c** period M
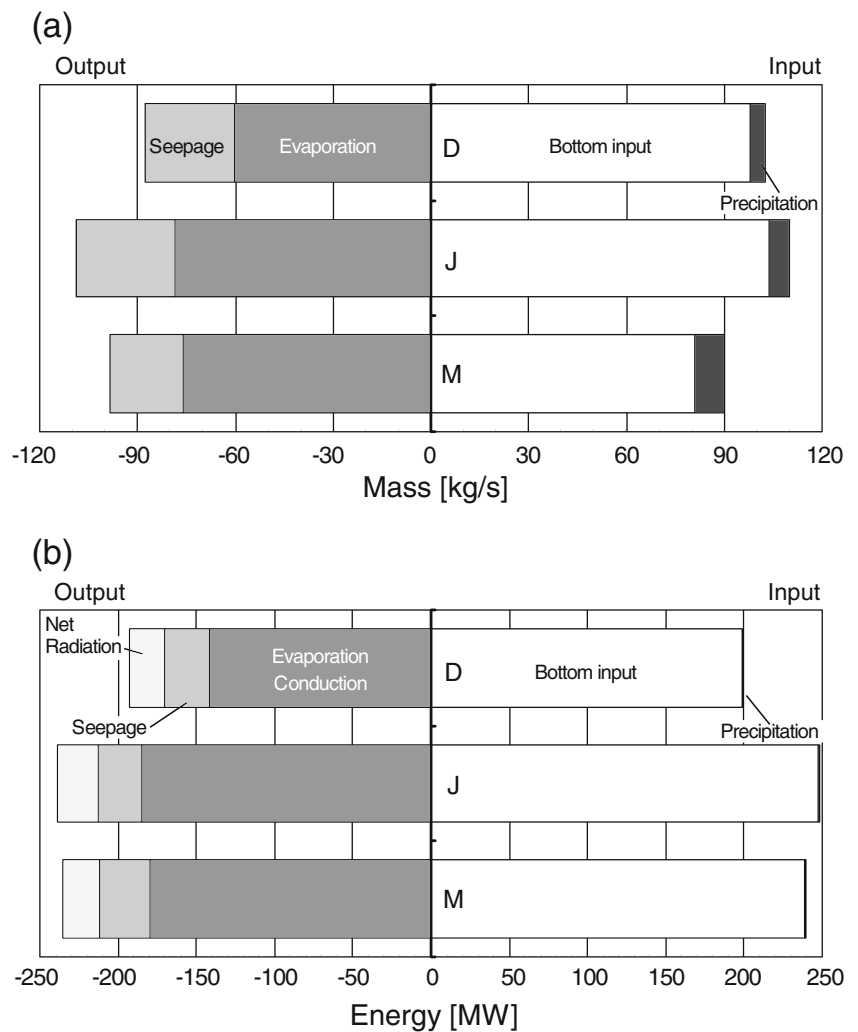
Fig. 8, which shows the average values for each period. The bulk of the mass supply at Yudamari is the bottom input fluid; precipitation inflows are negligible. The lake water is lost mainly by evaporation, followed by seepage. The bulk of the energy is supplied from the lake bottom; the energy is mostly released from the lake surface due to evaporation. The input and output energy are evenly balanced, meaning that the water temperature is designated by energy equilibrium.

Even if the energy equilibrium is maintained, it is not necessarily the case that the mass is balanced. During period D, the mass flux of the bottom input fluid exceeds the mass loss via evaporation and seepage (Fig. 8); consequently, the water level rises. In period J, the bottom input mass is balanced by the sum of evaporation and seepage loss (Fig. 8), meaning that the water level remains constant. During period M, the mass flux of the bottom input fluid is relatively small; however, its enthalpy is high (Fig. 8). Ultimately, evaporation output enhanced by high water temperature results in a decrease in water level.

Fluctuations in bottom input fluid

Figure 9 shows the time series of the optimal mass flux and enthalpy of the bottom input fluid. The data are plotted for the middle day within each period. The mass flux of the bottom input fluid varies between 75 and 132 kg/s, showing seasonal changes. The enthalpy of the bottom input fluid shows fluctuations, and it gradually increases from 1,840 kJ/kg at the end of 2006 to 3,030 kJ/kg at the end of 2008.

Figure 10 shows the estimated enthalpy plotted against the mass flux. The enthalpy decreases with increasing mass flux. Fluids with low enthalpy are supplied with a higher flux during summer and autumn, whereas fluids with high enthalpy are supplied with lower flux during winter and spring.

An important factor in estimating mass and enthalpy is evaporation loss because it is of the same order of magnitude as the bottom input fluid (Fig. 9). One of the main parameters that controls evaporation is wind speed (see Eq. 6). In the present analysis, we use 75% of the

Fig. 9 Temporal variations in **a** bottom input mass *m*, **b** bottom input enthalpy *H*, and **c** heat discharge rate (the product of *m* and *H*) during periods A–R. The periods indicated by meshes show rainy seasons
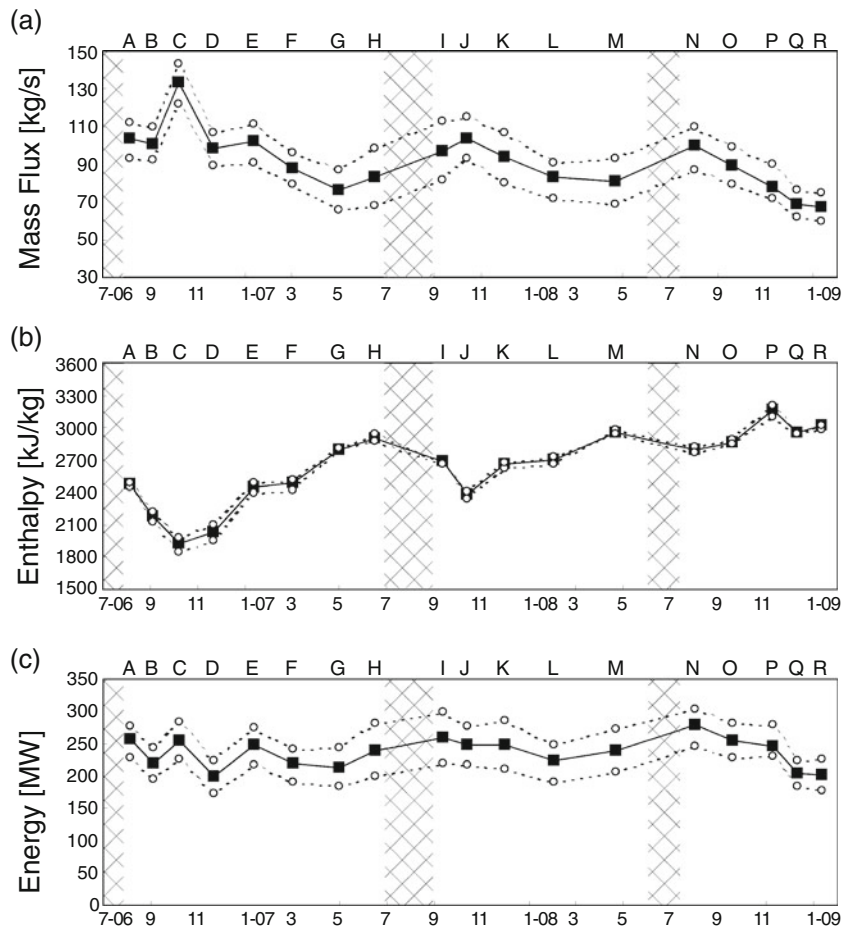
wind velocity recorded at AWS as the wind speed at the crater lake; however, it is important to assess the validity of this approach. We therefore assessed the estimation errors using 100% and 50% of the wind speed at AWS as the maximal and minimal limits, respectively (open circles in Fig. 9). A comparison with the results obtained using

Fig. 10 Relation between bottom input enthalpy and bottom input mass flux. *Letters* correspond to the periods shown in Fig. 2

75% of the wind speed at AWS reveals a largely systematic shift of less than ±12% in mass and ±5% in enthalpy; however, the signature of the fluctuation pattern remains. Although the estimates of mass and enthalpy include this degree of uncertainty, we consider that the uncertainty in wind speed does not preclude an interpretation of the mechanism that controls the supply of the bottom input fluid (see Discussion).
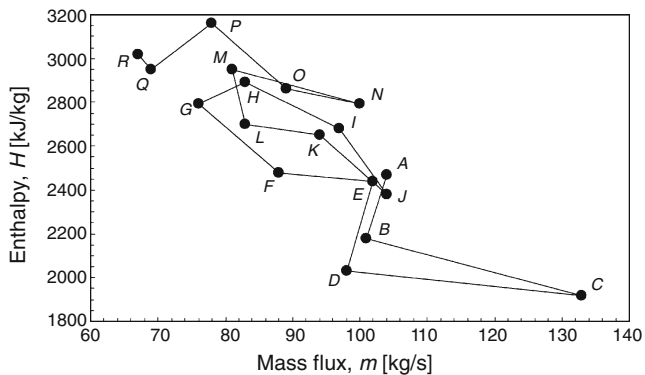
Discussion

A numerical model has been applied to the observation data obtained at Yudamari crater lake. At crater lakes such as Yudamari, it is possible to detect even slight changes in subaqueous geothermal activity. In contrast, evaluations of the energy emitted by subaerial fumaroles, or steaming ground, involve larger uncertainties, particularly when employing a remote sensing apparatus (Oppenheimer and McGonigle 2004). Here, we investigate the nature of the material emitted from the lake bottom.

Heat discharge from Yudamari crater lake

Figure 9c shows the rate of heat discharge from subaqueous fumaroles at Yudamari crater lake, calculated as the product of mass flux (Fig. 9a) and enthalpy (Fig. 9b). During the non-eruption period (periods A–R), the average heat discharge rate (190–260 MW) approaches the values for crater lakes Ruapehu (Hurst et al. 1991) and Poás (Brown et al. 1989), which are two of the most highest-discharge crater lakes in the world.

Historical documents record the repeated appearance and disappearance of Yudamari crater lake over the past 1,500 years, which indicates that the long-term heat discharge activity has occurred concomitantly with short-term fluctuations in the fluid supply, including eruptions. The average rate of magma discharge at Aso volcano over the past 90,000 years (during the post-caldera stage) is estimated to be ~1.5× 10^9 m³/ky (Miyabuchi 2009). This figure corresponds to a heat discharge rate of 150 MW, assuming a heat capacity of 1,000 J/kg/K, a latent heat of $4×10^5$ J/kg (Hardee 1980), a density of 2,600 kg/m³, and a temperature decrease of 800°C. The current heat flux carried by volatiles through Yudamari is comparable to the average heat based on magma discharge for the last 90,000 years.

Validity of estimated fluxes

As can be seen in Eq. 1, the validity of bottom input mass depends on the degree of uncertainty in accompanying seepage flux because calculations of water level are strongly dependent on the seepage term. To tie-up the loose ends, fluxes of other constituents besides H_2O, such as SO_2, can be used for indirect evaluation.

During periods A–R, our lake model estimates the high-temperature water vapor flux m_v as 46–71 kg/s, that is, 4,000–6,100 tonnes/day (see the following section for details). Assuming a SO_2/H_2O ratio in volcanic gas of 3 wt.% as representative of arc volcanoes (Poorter et al. 1991; Symonds et al. 1994), the corresponding SO_2 flux is 120–180 tonnes/day.

Meanwhile, the reported discharge rate of SO_2 was 200–400 tonnes/day (monthly report by JMA; based on their DOAS measurements), which is almost double the value above. The difference may be accounted by the additional SO_2 emission from the South wall fumaroles (SWFs, Fig.1), which is not relevant to our lake model. Unfortunately, the fraction of SWFs' contribution to the total SO_2 discharge is uncertain, though a measurement using a Raman Lidar (Nakamura et al. 2006) provides a hint. Those authors measured a horizontal profile of vapor phase H_2O over the first crater and revealed that the SWFs' contribution is 50–100% of the evaporative H_2O flux from the lake surface. Considering the SO_2/H_2O ratio does not

differ very much between the emissions from the SWFs and the lake surface, the SO_2 flux estimation from our model is not far from the realistic value, which confirms the general consistency of our calculations of water and heat budgets.

Origin of bottom input fluid

The bottom input enthalpy is estimated to be 1,840–3,030 kJ/kg (Fig. 9), which is much smaller than the figure of 6,000 kJ/kg estimated for the Ruapehu crater lake, suggesting that a heat pipe (Hurst et al. 1991) may not play an important role in the system at Yudamari crater lake. Assuming atmospheric pressure, the estimated enthalpy suggests that the bottom input fluid is either steam with a temperature of around 100°C, or simultaneous emissions of steam and liquid water. In addition, the relation between the enthalpy and mass flux (Fig. 10) indicates that the bottom input fluid is a mixture of high- and low-temperature fluids. The flux of low-temperature fluid changes through the years, while that of the high-temperature fluid shows only minor fluctuations.

We now consider the nature of the material that is emitted from the subaqueous fumaroles at Yudamari crater lake. The SWFs (Fig. 1a and b) have red-hot glows, suggesting the emission of high-temperature (>800°C) gas. Groundwater inflow has been observed at times when the crater bottom was deeply excavated due to volcanic explosions (Ikebe et al. 2008). The concentration of aqueous SiO_2 in the lake water is approximately 400 mg/L, which is greater than the saturating concentration of amorphous silica (Ohsawa et al. 2003), suggesting that part of the lake water is supplied from hotter water reservoirs.

Given the above, we consider that the bottom input fluid originates as a mixture of high-temperature volcanic gas and liquid water. To assess the mass fluxes of these components, we assume that the temperatures of steam and liquid water are 800°C and 100°C, respectively, meaning the specific enthalpy of steam H_v is 4,150 kJ/kg, and the specific enthalpy of liquid water H_w is 419 kJ/kg under an ambient pressure of $1×10^5$ Pa. The mass and energy conservation for each period are described by

$$m = m_v + m_w \tag{5}$$

$$mH = m_v H_v + m_w H_w \tag{6}$$

where m and H are the optimal bottom input mass flux and enthalpy estimated for each period (Fig. 9a and b), respectively, and m_v and m_w are the mass fluxes of high-temperature steam and liquid water, respectively.

Figure 11a and b shows the estimated m_w and m_v for each period, respectively. The temporal variations in m_w show annual cyclic changes (Fig. 11a) that increase from August to October each year, lagging 2 months behind the
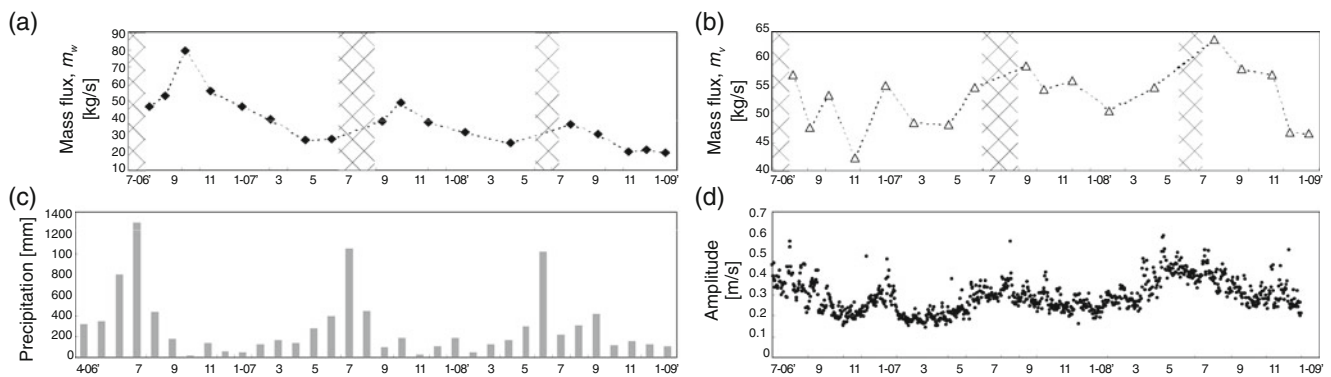
Fig. 11 Mass fluxes of liquid water m^w and high-temperature volcanic gas m^v, calculated based on Fig. 10a and b, assuming temperatures of 100°C and 800°C, respectively. See text for details. Temporal variations **a** in m^w and **b** in m^v. **c** Monthly precipitation measured at AWS. **d** Daily mean amplitude of a short-period seismometer deployed 600 m west of Yudamari (operated by JMA). The periods indicated by meshes represent rainy seasons

rainy season (June–July), which provides more than half the annual precipitation (Fig. 11c). The value of m_w after the rainy season in 2006 was relatively high compared with 2007 and 2008. The total rainfall during the rainy season in 2006 was 2,100 mm, whereas it was 1,200–1,400 mm in 2007 and 2008 (Fig. 11c). Therefore, we suspect that groundwater level coupled with precipitation during the rainy season reflects annual changes in the liquid water input to Yudamari, although with a time delay. The annual flux changes of groundwater with time delay are suggested by a ground temperature variation at a depth of 120 m that was recorded by a drill hole located 200 m west of Yudamari (KAF in Fig. 1a, Sudo and Hurst 1998).

The value of m_v shows apparent random fluctuations, although it is consistent with the fluctuations in the daily mean amplitude of velocity (Fig. 11d) measured at a permanent JMA short-period seismometer located 600 m west of Yudamari. Figure 11 indicates that the volcanic tremor recorded by the seismometer is enhanced by high-temperature volcanic gas.

Seismological studies indicate that the volcanic tremor observed around the first crater closely correlates with the ascent of volcanic gas from depth. Figure 11d shows two types of volcanic tremors; (1) isolated event-like tremor with a dominant frequency around 1 to 2 Hz, and (2) tremor with a dominant frequency around 3 to 10 Hz, which occurs continuously (Takagi et al. 2006). The isolated tremor (1) occurs beneath the SWFs (Fig. 1) at a depth of several hundred meters from the ground surface. The source mechanism of the tremor indicates that the ascent of volcanic gas from the crack-like conduit (Kaneshima et al. 1996, Fig. 12) enhance the isolated tremor (Yamamoto 2004; Mori et al. 2008). The source region of the continuous tremor (2) is located around the upper rim of the crack-like conduit (Fig. 12). Takagi et al. (2009) revealed that the source region and amplitude of the

continuous tremor changes with volcanic activity including phreatic eruptions, and they inferred that the continuous tremor is excited by the interaction between the volcanic gas and a low-temperature aquifer.

Water flow model beneath Yudamari crater lake

Figure 12 shows a schematic model of the transport of hydrothermal fluid at Aso volcano. Previous geomagnetic observations revealed that rapid heating and cooling occurred at depths of several hundred meters during the most recent eruptive period (1989–1990), suggesting the interaction of groundwater and superheated vapor in a shallow hydrothermal system (Tanaka 1993). More recently, magnetotelluric surveys have detected a significant low-resistivity region approximately 100 m below the crater lake. The upper part of this region is a hydrothermally altered zone, which is interpreted as a cap to upwelling fluids supplied from depth (Kanda et al. 2008). An analysis of the long-period tremor indicates that volcanic fluids are transported to the low-resistivity region through the crack-like conduit (Yamamoto et al. 1999) from depth. The source region of continuous tremor (2) is located close to the low-resistivity region, indicating the occurrence of fluid flow.

In this study we report a low enthalpy for the bottom input fluid, suggesting that both gas and liquid water ascend from the hydrothermal system beneath Yudamari. As in the case of Yudamari, simultaneous emissions of liquid water and steam are necessary at the Poás and Ruapehu crater lakes based on mass, energy, and Mg and Cl balances (Stevenson 1992). The system is similar to an analogue model that involves a two-phase boiling system, using a porous vertical cylinder saturated with water (Vandemeulebrouck et al. 2005). The base of the cylinder is heated and the top is cooled, as in a natural hydrothermal system.

Fig. 12 Schematic model of mass flow around the first crater of Nakadake, Aso volcano, during a non-eruption period. *Superscript numbers* refer to the following references: *[1]* Yamamoto et al. (1999); *[2]* Takagi et al. (2006); *[3]* Tanaka (1993); *[4]* Kanda et al. (2008); *[5]* Miyabuchi and Terada (2009); *[6]* Yamamoto (2004); and *[7]* Mori et al. (2008)
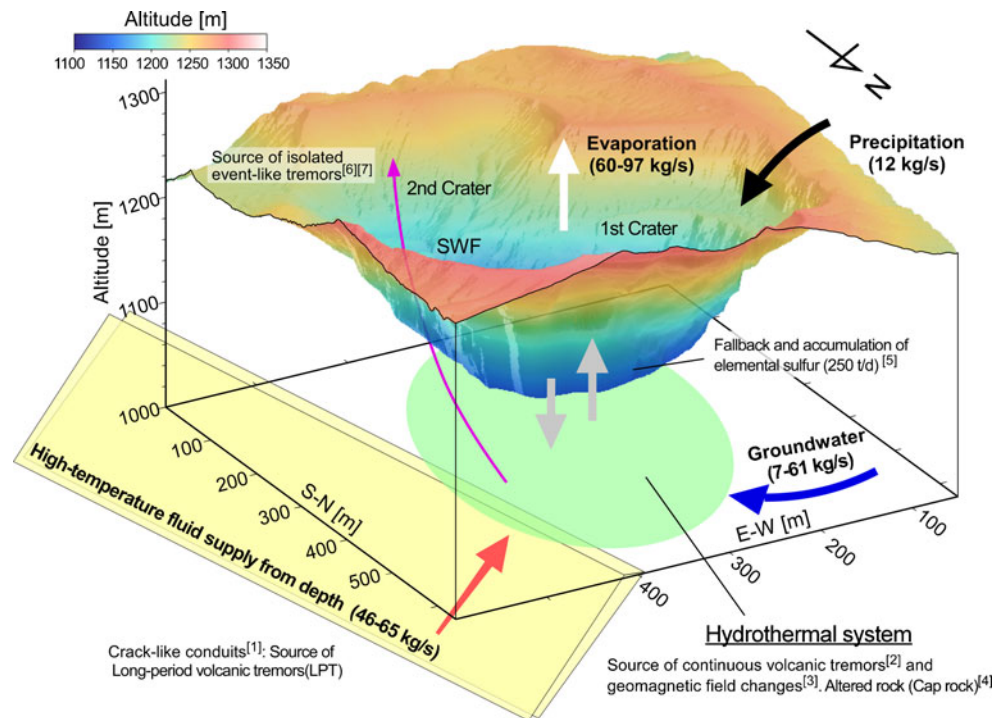
We consider that parameters of the hydrothermal system are controlled mainly by the mass balances of high-temperature steam input from depth, groundwater input (which has a seasonal flux), and seepage input (which depends on the lake level and surface area) to the system and output to the crater lake. Consequently, continuous observations of a hot crater lake are useful for inferring the variations of physical parameters (e.g., temperature and the mass ratio of gas to the liquid phase) in the underlying hydrothermal system.

Conclusions

A precise and continuous monitoring of water level and temperature was recently performed at Yudamari, Aso volcano. We observed characteristic patterns of change in lake level, including periods of mild rise (2.7–5.4 cm/day), plateau (change of less than ±1 cm/day), and mild decrease (1.4–2.7 cm/day), that show no direct correlation with precipitation. We developed a numerical model of a hot crater lake, applying it to precise observation data for July 2006 to January 2009, and we evaluated the temporal variations in the mass and enthalpy of the volcanic fluid supplied from the lake bottom. The mass flux shows seasonal changes within 75–132 kg/s, and its enthalpy shows minor fluctuations and a gradual overall increasing trend from 1,840 to 3,030 kJ/kg. Furthermore, the relation between the enthalpy and mass flux indicates

that the bottom input fluid is a mixture of high- and low-temperature fluids. We assumed that the subaqueous fumaroles emit both high-temperature steam (800°C) and liquid water (100°C), and we assessed the mass fluxes of these components. The liquid water flux shows a seasonal increase, lagging 2 months behind the rainy season, suggesting some of the liquid water is groundwater. The pattern of fluctuations in the flux of the high-temperature steam shows a relation with the amplitude of the volcanic tremor, suggesting that heating of the hydrothermal system drives the tremor. Consequently, continuous observations of a hot crater lake are useful in terms of inferring the variations of physical parameters in the underlying hydrothermal system.

APPENDIX: Expression for heat flux terms

The total heat flux from the lake surface Φ is expressed as the sum of evaporation φ_e, conduction φ_c, and net radiation φ_r:

$$\Phi = \varphi_e + \varphi_c + \varphi_r \tag{a1}$$

Evaporation is driven by free convection (due to the air–water temperature difference) and forced convection (due to horizontal wind). Hence, the evaporation heat flux depends on meteorological conditions such as vapor pressure e_a, virtual temperature T_{va}, and the wind speed u of ambient air. Ryan et al. (1974) formulated the total evaporation heat flux φ_e as

$$\varphi_e = \lambda(T_{vs} - T_{va})^{\frac{1}{3}}(e_s - e_a) + b_0 u(e_s - e_a) \tag{a2}$$

where λ and b_0 are empirical constants, 0.027 W/m^2/Pa/K$^{1/3}$ and 0.032 W/m^2/Pa/(m/s), respectively; e_s is the vapor pressure at the water surface corresponding to the saturation vapor pressure of water at the temperature; and T_{vs} is the virtual temperature at the water surface temperature. The virtual temperature T_v at temperature T is given by

$$T_v = T(1 + 0.608q) \tag{a3}$$

where q is specific humidity, a ratio of vapor density to air density.

Conduction heat losses φ_c are related to the evaporation flux by Bowen's ratio (Bowen 1926):

$$\varphi_c = B_o \varphi_e \tag{a4}$$

The parameter B_o is written as

$$B_o = C\frac{T_s - T_a}{e_s - e_a} \tag{a5}$$

where C is a constant of 61 Pa/K.

Radiation heat flux

The net radiation φ_r is expressed by

$$\varphi_r = R_{atm} + R_{sun} - R_{lake} \tag{a6}$$

R_{lake} is long-wavelength radiation from the lake surface,

$$R_{lake} = \varepsilon\sigma(T_s + 273.15)^4 \tag{a7}$$

where ε is water surface emissivity, 0.97; σ is the Stefan-Boltzmann constant, 5.67×10^{-8} W/m^2/K^4; and R_{sun} is short-wavelength solar radiation, which is assumed to be 115 W/m^2, corresponding to the yearly mean solar heat supply based on the data measured at Fukuoka and Kagoshima, located 100 km northwest and 150 km south

from Aso volcano, respectively (National Astronomical Observatory Japan 2000). Long-wavelength radiation from the atmosphere, R_{atm}, is represented by

$$R_{atm} = (208 + 6T_a)(1 + 0.0034C_l^2) \tag{a8}$$

where l is latitude, and C_l is the average cloud cover in oktas (Linacre 1992), as calculated by

$$C_l = 5.1946 - 0.23227l + 6.7727 \times 10^{-3}l^2 - 4.9495 \times 10^{-5}l^3 \tag{a9}$$

References

Abe M (1972) Studies on the water-balance in the Ikeda-Lake. Bull Fac Agric, Kagoshima Univ 22:1–80

Bowen IS (1926) The ratio of heat losses by conduction and evaporation from air water surface. Phys Rev 27:779–787

Brantley SL, Agustsdottir AM, Rowe GL (1993) Volcanic lakes reveal volcanic heat and volatile flux. GSA Today 3:173–178

Brown H, Rymer H, Dowden J, Kapadia P, Stevenson D, Barquero J, Morales LD (1989) Energy budget analysis for crater lakes: implication for predicting volcanic activity. Nature 339:370–373

Hardee HC (1980) Solidification of Kilauea Iki lava lake. J Volcanol Geotherm Res 7:211–223

Hurst AW, Bibby HM, Scott BJ, McGuinness MJJ (1991) The heat source of Ruapehu crater lake; deductions from the energy and mass balances. J Volcanol Geotherm Res 46:1–20

Ikebe S, Watanabe K, Miyabuchi Y (2008) The sequence and style of the 1988–1995 eruptions of Nakadake, Aso volcano, Kyushu, Japan. Bull Volcanol Soc Jap 53:15–33 (in Japanese with English abstract)

Iwamura K, Kaneshima S (2005) Numerical simulation of the steam-water flow instability as a mechanism of long-period ground vibrations at geothermal areas. Geophys J Int 163:833–851

Kanda W, Tanaka Y, Utsugi M, Takakura S, Hashimoto T, Inoue H (2008) A preparation zone for volcanic explosions beneath Nakadake crater, Aso volcano as inferred from electrical resistivity surveys. J Volcanol Geotherm Res 178:32–45

Kaneshima S, Kawakatsu H, Matsubayashi H, Sudo Y, Tsutsui T, Ohminato T, Ito H, Uhira K, Yamasato H, Oikawa J, Takeo M, Iidaka T (1996) Mechanism of phreatic eruptions at Aso volcano inferred from near-field broadband seismic observations. Science 273:642–645

Linacre E (1992) Climate data and resources. A Reference and Guide, Routledge

Miyabuchi Y (2009) A 90,000-year tephrostratigraphic frame work of Aso volcano, Japan. Sediment Geol 220:169–189

Miyabuchi Y, Terada A (2009) Subaqueous geothermal activity of acidic crater lake revealed by lacustrine sediments, Aso volcano, Japan. J Volcanol Geotherm Res 187:140–145

Mori T, Sudo Y, Tustsui T, Yoshikawa S (2008) Characteristics of isolated hybrid tremor (HBT) during a calm activity period at Aso volcano. Bull Volcanol 70:1031–1042

Nakamura T, Sugimoto N, Tsuda T, Abo M, Hashimoto T, Terada A (2006) Observation of water vapor with a portable Raman Lidar—continuous monitoring and filed experiment over the forest and at the volcano. Reviewed and revised papers, 23rd International Laser Radar Conference 2006, Part ll:897–900

Nakao K, Otsuki S, Tanouoe R, Naruse R (1967) Watershed Leakage from the Closed Lake Lake Kuttara. Geophys Bull Hokkaido Univ 17:47–64

National Astronomical Observatory (2000) Rika nenpyo (chronological scientific tables). Maruzen Co., Ltd., Tokyo

Ohba T, Hirabayashi J, Nogami K (1994) Water, heat and chloride budgets of the crater lake Yugama at Kusatsu-Shirane volcano, Japan. Geochemical J 28:217–231

Ohsawa S, Sudo Y, Mawatari H, Shimoda G, Utsugi M, Amita K, Yoshikawa S, Yamada M, Iwakura K, Onda Y (2003) Some geochemical features of Yudamari Crater Lake, Aso volcano, Japan. Geotherm Res Rep Kyushu Univ 12:62–65 (in Japanese with English abstract)

Oppenheimer C (1997) Ramifications of the skin effect for crater lake heat budget analysis. J Volcanol Geotherm Res 75:159–165

Oppenheimer C, McGonigle AJS (2004) Exploiting ground-based optical sensing technologies for volcanic gas surveillance. Ann Geophys 47:1455–1470

Pasternack GB, Varekamp JC (1997) Volcanic lake systematics I. Physical constraints. Bull Volcanol 58:528–538

Poorter RPE, Varekamp JC, Poreda RJ, Bergen MJV, Kreulen R (1991) Chemical and isotopic compositions of Volcanic gases from the east Sunda and Banda Arcs, Indonesia. Geochimica et Cosmochimica Acta 55:3795–3807

Rouwet D, Yuri T, Nicholas RV (2004) Dynamics and mass balance of El Chicho'n crater lake, Mexico. Geofisica Internacional 43:427–434

Rowe GL, Brantley SL, Fernandez M, Fernandez JF, Borgia A, Barquero J (1992) Fluid-volcano interaction in an active stratovolcano; the crater lake system of Poás volcano, Costa Rica. J Volcanol Geotherm Res 49:23–51

Ryan PJ, Harleman DR, Stolzenb KD (1974) Surface heat loss from cooling ponds. Water Resour Res 10:930–938

Saito T, Ohsawa S, Hashimoto T, Terada A, Yoshikawa S, Ohkura T (2008) Water, heat and chloride balances of the crater lake at Aso volcano, Japan. J Geotherm Res Soc Japan 30:107–120 (In Japanese with English abstract)

Stevenson DS (1992) Heat transfer in active volcanoes—models of crater lake systems, PhD thesis, Open University, Milton Keynes, UK

Sudo Y, Hurst AW (1998) Temperature changes at depths to 150 metres near the active crater of Aso volcano: preliminary analysis of seasonal and volcanic effects. J Volcanol Geotherm Res 81:159–172

Symonds RB, Rose WI, Bluth GJS, Gerlach TM (1994) Volcanic gas studies—methods, results, and applications. Rev Mineral 30:1–66

Takagi N, Kaneshima S, Kawakatsu H, Yamamoto M, Sudo Y, Ohkura T, Yoshikawa S, Mori T (2006) Apparent migration of tremor source synchronized with the change in the tremor amplitude observed at Aso volcano, Japan. J Volcanol Geotherm Res 154:181–200

Takagi N, Kaneshima S, Ohkura T, Yamamoto M, Kawakatsu H (2009) Long-term variation of the shallow tremor sources at Aso volcano from 1999 to 2003. J Volcanol Geotherm Res 184:333–346

Tanaka Y (1993) Eruption mechanism as inferred from geomagnetic changes with special attention to the 1989–1990 activity of Aso volcano. J Volcanol Geotherm Res 56:319–338

Terada A, Yoshikawa S (2009) Development of observation techniques for inaccessible and extremely acidic crater lakes: installation of temperature telemetry buoys, dredging of lake sediments, and sampling of lake waters. J Geotherm Res Soc Japan 31:117–128 (in Japanese with English abstract)

Terada A, Hashimoto T, Kagiyama T, Sasaki H (2008) Precise remote-monitoring technique of water volume and temperature of a crater lake in Aso volcano, Japan: implication for a sensitive window of volcanic hydrothermal system. Earth Planets Space 60:705–710

Vandemeulebrouck J, Stemmelen D, Hurst T, Grangeon J (2005) Analogue modeling of instabilities in crater lake hydrothermal systems. J Geophys Res 110 doi:10.1029/2003JB002794

Yamamoto M (2004) Volcanic fluid system inferred from broadband seismic signals. PhD thesis, University of Tokyo, Japan

Yamamoto M, Kawakatsu H, Kaneshima S, Mori T, Tsutsui T, Sudo Y, Morita Y (1999) Detection of a crack-like conduit beneath the active crater at Aso volcano, Japan. Geophys Res Lett 26:3677–3680